VARIETY OF SPECTRAL SIGNATURES OF LITHICS WITHIN THE NORTH POLAR LAYERED DEPOSITS ON MARS. P. Sinha and B. Horgan, Purdue University (sinha37@purdue.edu).

Introduction: The North Polar Layered Deposits (NPLD) of Mars are up to 3 km thick ice-rich sedimentary deposits that form the north polar plateau, Planum Boreum (PB). Climate models for modern Mars predict that the NPLD accumulated over the last few million years during periods of low obliquity when seasonal deposition of frost/ice trapped dust and other sediments [1,2]. The NPLD are a record of the recent climatic history of Mars analogous to terrestrial ice sheets preserving records of Earth's recent climate. The 2011 NRC Planetary Science Decadal Survey identifies the NPLD as a high priority target and recommends a robotic mission to sample ice core for climatic records. Linking the NPLD to climatic history will require quantitative age-dating of ice. Because old ice loses the annual layers and trapped gases that are used to date younger ice, older ice cores on Earth are dated via K-Ar radiometric dating of lithic materials such as volcanic ash layers [3]. However, the non-ice composition of the NPLD is poorly characterized and mostly assumed to be airfall martian dust, which is not dateable. Mafic minerals are present in the north polar erg surrounding the NPLD, which appears to source some sediments from the polar plateau [4]. Dark sedimentary veneers inconsistent with light-toned dust have been observed mantling regions within the NPLD but their composition remains unknown [5]. In this study, hyperspectral data from Compact Reconnaissance Imaging Spectrometer for Mars (CRISM) is used to investigate the composition of lithic sediments within the NPLD. The mineralogical detections will be key to constraining sediment sources, transport processes, and determining whether or not the NPLD contain the materials for quantitative geochronology.

Methods: CRISM TRR3 Full Resolution Targeted (FRT) and Half Resolution Long (HRL) images were analyzed using the ENVI CRISM Analysis Toolkit (CAT). These 18-40 m/pixel hyperspectral VNIR (0.35-2.65 μm) images are corrected for photometric and atmospheric effects. Fe-bearing minerals cause a broad absorption near 1 μm and often also near 2 μm [6-8]. Olivine exhibits a broad absorption centered between 1.05-1.07 μm, pyroxene exhibits bands centered near 0.9-1.05 μm and 1.9-2.4 μm, while Fe-bearing glass has relatively broader, shallow and symmetric bands centered between 1.08-1.16 μm and a weaker absorption band around 2.0 μm (Fig. 1). The absorption bands for glass are resolvable only when glass is present in high abundances (>~70%) but can be detected as a distortion on other mineral bands at moderate abundances (>~50%) [4]. Most previous glass detections in the region are also associated with a spectrally featureless strong blue and concave up slope which is interpreted as weathering of the glass surface [9].

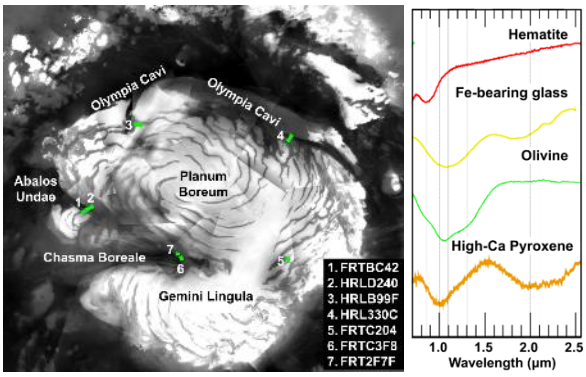

Figure 1: *(Left) NPLD sites in this study over MOC atlas. (Right) Lab spectra of NPLD-relevant mafic minerals.*

Spectral summary parameters are used to generate RGB maps of spectral variations to identify regions of interest (ROIs) for spectral analysis [9]. To suppress surface dust and water ice, we ratio the ROI spectrum by calculating a reference spectrum from an average of pixels from the same detector column in the scene displaying a high value for spectral parameter BD530 (ferric dust), lower values for parameters BDI1000VIS and HCPINDEX2 (mafics) and with a water ice band depth at 1.5 μm similar to the selected ROI. This process is effective in revealing the mineralogy of lithic materials. To clearly see the broad Fe-absorption bands near 1 μm and 2 μm, the continuum of each spectrum is then suppressed by dividing the ratio spectrum by a linear convex hull continuum shape [6,10-11]. Band centers were determined using the methods of [6]. Due to hydration bands and residual atmospheric bands, 1.85-2.15 μm was replaced with a polynomial fit for band analysis.

Results: Seven CRISM images were analyzed to constrain the lithic composition of the NPLD (Fig. 1). The strongest mafic signatures in ratio spectra are bands centered between 0.97-1.10 and 2.03-2.17 μm, where bands closer to 1.00 and 2.15 μm are consistent with high-Ca pyroxene (HCP). Bands at 1.07-1.10 μm could be consistent with either glass or olivine, but these spectra often exhibit bands closer to 2.00 μm that are more consistent with glass. In cases where these spectra do not exhibit a 2 μm band, strong rounding of the band, and the lack of a 1.3 μm shoulder are more consistent with a highly reduced Fe-bearing glass than olivine [12].

PB1 (ABb_1) forms most of the NPLD and contains thousands of meter-scale horizontally stacked ice-rich layers. This unit is generally red sloped with absorptions at 1.5 and 2.0 μm suggesting that ABb_1 is dominated by water ice and ferric dust [13-15]. Upon ratioing, some spectra exhibit glass-like absorptions (Fig. 2a). PB-2 (ABb_2) is a dark-toned sedimentary unit which heterogeneously overlays ABb_1, and also mantles the floor of Chasma Boreale and Olympia Cavi. ABb_2 generally

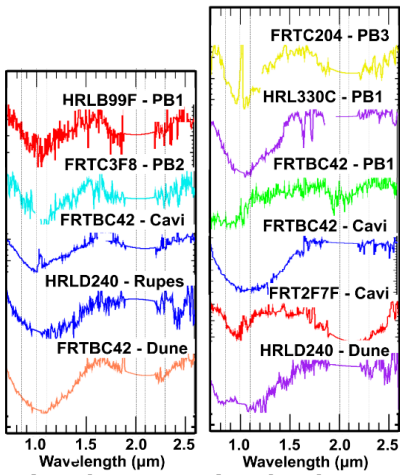

Figure 2: *(a, left) Representative continuum removed spectra. and (b, right) spectral variability of lithic units in the NPLD.*

exhibits a strong blue and concave up slope with weak iron absorptions consistent with weathered glass (Fig. 2a). ABb_1 and ABb_2 are overlain by the PB3 (ABb_3) unit, a young residual ice cap dominated by ice. Below the NPLD, the Cavi unit (ABb_c) is a thick dark unit with some light toned beds that are deformed, eroded, and sometimes discontinuous. ABb_c is spectrally dominated by varying mixtures of weathered and unweathered glass with HCP (Fig. 2a). The base of PB exposes the Rupes (ABb_r) unit, which shows a broad absorption at 1.1 μm and negligible absorption at 2 μm, consistent with glass. Dunes surrounding the NPLD appear to source the sandy material by eroding the Cavi unit. The sand in the dunes at Abalos Undae shows a broad absorption around 1.1 and 2.1 μm indicating it to be glass-rich mixture containing HCP (Fig. 2a).

However, additional spectral variability is present within the lithic units in the NPLD (Fig. 2b). For example, ABb_1 is mostly glassy, however, signatures consistent with minerals like olivine, pyroxene, hematite, etc. have also been detected. Absorption at 0.86 μm consistent with hematite is sometimes detected in dune sands. Finally, weak HCP signatures have been detected at some locations within the residual ice cap ABb_3.

Discussion: A major finding of the study is that along with airfall martian dust (spectrally dominated by nanophase ferric oxide [16]) other lithic materials such as glass, pyroxene, and olivine are present within the NPLD [17-19]. ABb_3 is the uppermost ice-rich layer, which appears less dusty and contains a small fraction of lithics. These sediments may be reworked material from ABb_1 (e.g., eroded during trough migration), or a distinct sedimentary layer. ABb_1 consists of highly dusty layers with occasional glass signatures. ABb_2 is usually exposed at the periphery of the NPLD, has a low ice content, and is covered with low albedo sediment consistent with weathered glass. This unit may represent a discrete sedimentary layer or a sublimation lag [5,20]. The sand-rich Cavi (ABb_c) unit below ABb_1 is interpreted as an indurated sand sea and contains HCP in a variable mixture of weathered and unweathered glass. The dark-toned basal unit, Rupes, is the oldest unit, interpreted as reworked sediments from the surrounding plains of Vastitas Borealis, and exhibits only glassy signatures.

There is compositional similarity between lithic materials within and around the NPLD, however, it is unlikely that the NPLD lithics are sourced from the surrounding plains. Wind models suggest that katabatic winds drive transport down off the cap and not up onto it [21], so sediment is more likely to be emplaced on the NPLD either ballistically or via atmospheric fallout. Compositional similarities to the surrounding plains may thus be due to deposition of same mantling unit, or the NPLD could be a source of sediments for the plains due to erosion by katabatic winds. In addition, possible detection of olivine within the NPLD suggests that materials are sourced from far distances, since olivine is not found in the surrounding plains within 1000 km.

Two likely sources for NPLD sediments are impact ejecta or volcanic eruptions, suggesting that the NPLD records impactor flux and eruption rates in addition to climate. Proximal impact ejecta would contain a large fraction of local country rock and small amounts of impact glasses which decrease in grain size with distance from the impact, while distal impacts globally distribute a layer mm to tens of cm thick sand-sized spherules and larger tektites that are typically glassy but can be crystalline based on its cooling history [17,22-24]. Volcanic tephras range from crystalline to glass-rich, where glass abundances are significantly enhanced by water/ice interactions during eruption [25]. Climate models suggest that only the finest-grained volcanic ash can be latitudinally transported from the mid-latitudes to poles [19], so sands in the NPLD may be more likely to be impact in origin. In either case, these sediments could provide both compositional markers for correlation of relative stratigraphies across the region, as well as potential sediments for quantitative geochronology.

References: [1] Pollack & Toon (1982) Icarus 50, 259. [2] Becerra et al. (2016) JGR 121, 1445. [3] Basile et al. (2001) JGR 106, 31915. [4] Horgan & Bell (2012) Geology 40, 391. [5] Rodriguez & Tanaka (2007) Mars 1, 15. [6] Horgan et al. (2014) Icarus 234, 132. [7] Minitti et al. (2007) JGR 112, 1-24. [8] Cloutis et al. (1990) Icarus 86, 383. [9] Viviano-Beck et al. (2014) JGR 119, 1403. [10] Bennett et al. (2016) Icarus, 273, 297. [11] Greenhagen et al. (2010) *Science*, *329*, 1507. [12] Cannon et al. (2017) *JGR 122*, 129. [13] Tanaka et al. (2008) Icarus 196, 318. [14] Tanaka & Fortezzo (2012) USGS SIM 3177. [15] Smith & Holt (2015) JGR 120, 362. [16] Ehlmann et al. (2017) JGR 122, 2510. [17] Lorenz (2000), Icarus 144, 353. [18] Schultz & Mustard (2004), JGR 109(E1). [19] Kerber et al. (2012) Icarus 219, 358. [20] Massé et al (2010) Icarus 209, 434. [21] Smith & Spiga (2017) Icarus *308*, 188. [22] Liu et al. (2009) GSA SP 452, 37. [23] Glass (2016) Int J Appl Gl Sci, 7(4), 435. [24] Johnson & Melosh (2013) Nature 485, 75. [25] Wall et al. (2014) Nat Com 5, 5090.